ORIGINAL PAPER

Thermal and mechanical properties of poly(lactic acid) filled with modified silicon dioxide: importance of the surface area

I. Montes-Zavala, et al. *[full author details at the end of the article]*

Abstract

In this research work, the effect of the change in the surface area of silicon dioxide nanoparticles of the same size on mechanical properties of poly(lactic acid) nanocomposites (PLA) was studied, as well as the role of coupling agent amount in the compatibility of these nanomaterials. We consider a spherical silicon dioxide with a surface area of 170–200 m^2/g (labeled as S–SiO_2) and another considered amorphous with a surface area of 180–600 m^2/g (labeled as P-SiO_2). This surface areas difference plays an important role in modifying of nanoparticles polarity by incorporating a coupling agent and its integration into partially polar polymers. According to obtained results, for nanomaterials with high surface area, it was observed while increasing coupling agent amount, the elasticity of the composite was observed to increase. In contrast, in nanomaterials with spherical nanoparticles, it was observed that as the amount of coupling agent decreases, the resistance of the material increases, reaching a maximum when a 10:2 ratio is used. It was observed that behaviors for both nanoparticles were different, which gives an idea that the incorporation of nanoparticles in polymers is not an issue of coupling agent or quantity only, it is more important as it is arranged on the surface. This kind of couplings does not only affect mechanical properties, since the thermal behavior of the material was also influenced, where it was observed that particles with low surface area modify the crystallization rate when they have different percentages of coupling agent on the surface. Furthermore, it is observed that the incorporation of nanoparticles with high surface areas area does not modify the crystallization rate significantly. Besides, in both cases, it was observed that the highest crystallization rate is reached when a 10:2 ratio is used. However, the energy required to form crystals remains unchanged. Therefore, it is considered that the incorporation of nanoparticles only affects the crystal formation rate without disturbing the energy requirement for crystal formation. Finally, a maximum in the 10:2 ratio was observed for the compatibility in both particles, which was manifested in an increase in the storage module through a dynamic mechanical analysis. The rate of crystal formation

I. Montes-Zavala, M. J. Pérez-González authors contributed equally.

as well as the number of formed crystals have a considerable effect on mechanical properties of nanocomposites when the surface area is modified.

Keywords Poly(lactic acid) · Mechanical properties · Nanocomposites · Non-isothermal crystallization

Introduction

In the past decades, the use of conventional materials such as metals has been involved in several daily life applications. However, nowadays we have looked for ways to incorporate polymers to replace conventional materials. The advantage of using polymers is their processability, low cost and productivity. However, one of its disadvantages are its mechanical properties; so it is necessary to incorporate a filler to improve them. This is because they need to have a high strength/high Young's modulus depending on the application that is going to be given [1].

The current tendency is to replace petroleum-derived polymers with materials coming from renewable sources and friendly to the environment. Poly(lactic acid) (PLA) is a polyester made of block 2-hydroxypropionic acid. It is known to be a compostable and biodegradable thermoplastic that derives from renewable sources such as sugar where the PLA is obtained [2]. The use of PLA has been relevant due to its applications in food packaging and is widely used in the biomedical field. Recently it has had an important participation due to its potential to replace oil derivatives [3]. The PLA has low mechanical properties and to improve PLA properties, fiber glass has been used as filler to increase its stiffness to double and 3 times its impact resistance using 20% fiberglass [4]. In addition, it has been tested with natural cellulose fibers to enhance mechanical performance by 42% when 20% fibrous material is used. This result showed that applications of PLA can be issued to manufacture materials that resist high temperatures [5]. Carbonaceous material blends with fibers have been involved in the modification of PLA nanocomposites, highlighting the betterment of poly(lactic acid) compatibility with the filler and resulting in an increase in mechanical and thermal properties [6]. Studies on improving the thermal stability and crystallinity of PLA have also been conducted using reactive copolymers such as synthesized PSMG and PSG. In case of the PLA molecular weight spotlight, it increases significantly with the addition of these copolymers and the PLA crystallization behavior is strongly influenced by the copolymer chains [7]. Ternary PLA blends nanocomposites have been studied to set forth new types of nanomaterials with good mechanical, thermal and bactericidal properties.

Metal oxides have been used as fillers to modify poly(lactic acid) nanocomposites and to increase their range of applications. Mainly, applications that have had these modifications are approached on the food packaging area. This is because in modern life its protection is essential and guarantees the quality of the product during transport to distant places [8]. Recently, zinc oxide nanoparticles (ZnO NPs) have been included to enhance some important properties in food packaging, such as UV light barrier, water vapor barrier and antibacterial properties. The ZnO NPs incorporation

improved the water vapor barrier and mechanical properties but its thermostability decreased [9]. Mechanical and thermal properties are important in engineering applications. However, plenty of the problem of nanoparticles incorporation into polymeric matrices is their dispersion. Therefore, SiO_2 systems have been carried out with superficial modifications to study the dispersion effect on PLA properties. It has been observed that the nanoparticles dispersion shows improvements in the crystallization rate and PLA crystallinity due to surface energy and interfacial energy between nanoparticles and the lateral crystals surface [10]. A coupling agent which has been involved in modifying the dispersion of SiO_2 nanoparticles is 3-aminopropyltriethoxysilane (3-APTES). Although the 3-APTES use is complex due to its multilayer deposition and the irregular morphology that it generates, it is extensively used to modify the metal oxide nanoparticles surface charge and improve its stability in solvents and polar matrices [11–13]. A recently study demonstrated that the chemical modification of metal oxides (as TiO_2) with aminosilanes has a direct effect on the non-isothermal crystallization of the PLA; mainly in the rate at with which PLA chains are accommodated in the first steps [14]. Besides, modifying the surface charge using 3-APTES has been important for carbon dioxide adsorption on mesoporous silica, which can be extended to the gas selective films manufacture [15]. A similar aminosilane to 3-APTES used for surface modification is 3-aminopropyltrimethoxysilane (3-APTMS) which is employed by its adhesion promotion. The 3-APTMS molecule has three methoxy groups and is able to polymerize in the presence of water [16]. A study showed that the reactivity with the silicon oxide layer and the polymerization process of aminosilanes depend on the number of possible bonding sites and the 3-APTMS reacted the most intensively with the silicon dioxide compared with others aminosilanes [17]. Also, the modification of the silicon dioxide surface by 3-APTMS strongly depends on the type solvent used. Results of a study showed that ethanol forms thin 3-APTMS coatings on silicon dioxide surfaces [16].

The understanding of PLA crystallization behavior is crucial for the control of its degradation rate, thermostability, mechanical, barrier properties and crystal nucleation kinetics [18, 19]. Studies on PLA non-isothermal crystallization include nanoclays and linear low-density polyethylene (LLDPE) where the results indicate that the nanoclays presence improves the PLA crystallization in heating, as well as the plasticizer (LLDPE) presence improves the PLA chains mobility [20], this phenomenon of facilitating the PLA chains mobility due to another polymer embedded has also been observed previously in PET/PLA blends [21]. There are different strategies to promote crystallinity in order to increase the PLA crystalline content. That is, through the heterogeneous nucleation effect, the PLA chains mobility increases. There are studies where it has been tested by adding above 10% acetyl triethyl citrate in PLA matrices obtaining good results [22]. However, particle size of filler has a share in the crystallization process; micro-sizes improve the crystallization rate and PLA growth rate while a large nanometric particles number retard the crystal initial growth, probably due to PLA molecules reduced its mobility [23]. Other PLA non-isothermal studies with various additives indicated that polysaccharides can be used as cheap fillers without changing the PLA crystallization [24]. An effect bit studied on transport and PLA relaxation properties is the nanoparticles morphology that are

incorporated into the matrix. When spherical and rod-shape zinc oxide morphologies are used as fillers in PLA matrices, high agglomerate formation occurs when the spherical shape is used. While rod-shaped morphology maintains a better dispersion that also improves PLA optical properties [25].

Among variables that mainly affect mechanical and thermal properties are the nanostructure morphology, agglomerates formation in the polymer matrix and the coupling agent amount on the metal oxide surface. Even when the same particle size is used, the results reported by each research group present contrasts. This research seeks to demonstrate that not only the particle size but also the surface area has an important role in the mode that the polymer chains interact with the nanoparticles. Two silicon dioxides (SiO_2) with different surface area and similar particle size were used with 3-APTMS organic coating to modify the metal oxide surface and avoid aggregates formation in a PLA matrix. Modifications were made in the coupling agent amount on the surface to observe the coating effect on the PLA/SiO_2 nanocomposite behavior and improve PLA mechanical properties without influence its thermal properties.

Materials and methods

Materials

To prepare PLA/SiO_2 nanocomposites, commercial PLA (3D Market, 3 mm) and silicon dioxide nanoparticles supplied by US Research Nanomaterials Inc were used. In this work, two surface areas were employed. It was used SiO_2 (99.5%, 15–20 nm, S- type, spherical, 170–200 m^2/g) labeled as S-SiO_2 and SiO_2 (99%, 20–30 nm, 180–600 m^2/g) labeled as P-SiO_2. Additionally, distilled water, (3-aminopropyl) trimethoxysilane, chloroform provided by J. T Baker and Petri dishes were employed.

Chemical modification of SiO₂ nanoparticles

SiO_2 nanoparticles were modified superficially by a silanization process. The coupling agent was added in different proportions, SiO_2:APTMS, (10:4, 10:2, 10:1) for 2 nanoparticles types. The proportions and specific surface area measured by N2-BET method are shown in Table 1. For the incorporation of SiO_2 nanoparticles in the ethanol for all experiments, 30 min of agitation in magnetic stirring were used, with 30 min of sonication at 60 Hz in an ultrasonic bath, until a total of 2.5 h were completed. Subsequently, the (3- Aminopropyl) trimethoxysilane was added, and at 10-min intervals, 1 ml of water was added to promote hydrolysis in the reaction, stirring at 400 rpm for 6 h. The suspension was washed by centrifugation twice with water and five time with methanol at 300 rpm for 10 min per wash, in order to remove the unreacted agents. The drying was carried out in an oven at 80 ℃. The dry powders were stored in vials for further testing.

Table 1 Coupling agent ratio used on silicon dioxide surface

Type	Sample	SiO$_2$ (g)	APTMS (ml)	Specific Surface Area (m^2/g)
S-SiO$_2$	**M1**	10	4	220
	M2	10	2	203
	M3	10	1	214
P-SiO$_2$	**M4**	10	4	382
	M5	10	2	368
	M6	10	1	296

Z potential and size particle

The particle size distribution as well as obtaining the Z potential of different modified SiO$_2$ samples was performed on a Delsa Nano C Particle Analyzer (Beckman Coulter). For particle size samples, modified SiO$_2$ samples were suspended in water. While for Z potential test, the pH was varied from 3 to 11, in order to monitor the modified SiO$_2$ nanoparticles behavior.

Nuclear magnetic resonance of modified SiO$_2$ nanoparticles

^{29}Si NMR and ^{13}C NMR spectra were obtained in a Bruker Ascend (400 MHz) instrument operating at 400 (^{29}Si) and 100 (^{13}C) MHz. For ^{13}C analysis, parameters were a scan number (NS) of 16 and a pulse length of 8.5 microseconds.

Scanning electron microscopy and surface area analysis

An EVO HD LS Zeiss electron microscope was used to obtain SiO$_2$ nanoparticle micrographs. In addition, an EDS X-MaxN X-ray detector was used to obtain the X-ray scattering data. To correctly measure the SiO$_2$ samples, the SiO$_2$ nanoparticles were previously coated with a gold plating, because the nanoparticles contain an organic coupling agent on the surface. The surface area of the modified SiO$_2$ samples was determined by the N$_2$-BET method using a surface area and porosimetry analyzer, Micromeritics, ASAP 2010.

Preparation of PLA/SiO$_2$ nanocomposites

A ratio of 1% modified SiO$_2$ nanoparticles in PLA was used for the production of films. First, a quantity of poly(lactic acid) was dissolved in sufficient chloroform, modified SiO$_2$ nanoparticles were added, and the system was stirred and sonicated constantly to assure mixture. Subsequently, suspensions were placed in

Petri dishes and kept in a controlled environment at room temperature to keep the evaporation of the solvent as homogeneous as possible.

Non-isothermal crystallization of PLA/SiO$_2$ nanocomposites

Non-isothermal crystallization was carried out on a TA instruments model Q2000 differential scanning calorimeter (DSC) in a dry nitrogen atmosphere. About 5 mg of the samples were melted at 200 ºC and held for 10 min to erase the thermal and mechanic memory and were then cooled at constant rates of 2.5, 5, 10 and 20 ºC/min. The exothermal curves of heat flow as function of temperature were also recorded to analyze the crystallization process.

Non-isothermal crystallization kinetics

In accordance with Avrami equation, this considers a constant crystallization rate temperature, then we have following Equation

$$X_t = 1 - e^{Z_t t^n} \tag{1}$$

where X_t represents the degree of relative crystallization, the exponent n refers to a constant mechanism and its value is subject to a type of nucleation and growth process parameters. Z_t represents composite rate constant, which involves nucleation and growth parameters, and the crystallization time is represented by t. Assuming differential crystallization changes, the relative crystallization is represented by Eq. 2

$$X_t = \frac{\int_{t_0}^{t} \left(dH_c/dt \right) dt}{\int_{t_0}^{t_\infty} \left(dH_c/dt \right) dt} * 100 \tag{2}$$

The time at the onset and end of the crystallization process is represented by t_0 and t_∞, respectively. Differential enthalpy changes are symbolized by dH_c and these are integrated in a time range. With the crystallinity and time data, Z_t and n parameters were calculated using a fit in Eq. 3. The fit was obtained changing to a double logarithmic form:

$$\log \left(-\ln \left(1 - X_t \right) \right) = \log \left(Z_t \right) + n \log \left(t \right) \tag{3}$$

Assuming a non-isothermal character of analyzed process, the Z_t parameter from Jeziorny's model shows a dependence with the cooling rate, ɸ. This suggests the non-isothermal crystallization can be represented by equation:

$$\ln \left(Z_c \right) = \ln \left(Z_t \right) / \varphi \tag{4}$$

As a result to consider the non-isothermal process as small isothermal steps, this fact is modeled by the Ozawa Equation:

$$1 - X_t = e^{-K(T)/\varphi^m} \tag{5}$$

The cooling function is represented by the term K(T), the Ozawa exponent is symbolized by *m*, the crystal growth depends on this exponent. Unfortunately, Avrami and Ozawa equations are inconvenient to analyze the non-isothermal crystallization process of polymeric systems. For a certain values of crystallinity degree, both the Avrami and Ozawa equation (Eq. 1 and Eq. 5, respectively) can be combined to produce another non-isothermal analysis. The combined model is known as model of Mo, and it is represented by the follow equation:

$$\ln(\varphi) = \ln(F(T)) - a\ln(T) \tag{6}$$

and

$$F(T) = \left[K(T)/Z_t\right]^{1/m} \tag{7}$$

The cooling rate to reach a crystallinity degree at unit crystallization time is represented by F(T). The *"a"* parameter corresponds to coefficient of Avrami's and Ozawa's exponent, i.e., $a = m/n$.

The crystallization phenomenon is evaluated through the change in the activation energy, the mathematical method of Kissinger [26, 27] has been widely used in this process. This method correlates changes of the crystallization peak temperature as a function of the cooling rate obtained by a fitted value of ΔE. However, the method has evidenced that the Kissinger equation is mathematically inapplicable to quantify activation energy of processes that occur upon cooling [28]. Friedman and Vyazovkin [28, 29] proposed an isoconversional method to determinate the correct behavior of ΔE. In this research work, the Friedman method [30] was used to calculate the effective activation energy. Besides, it was studied as a function of the degree of crystallinity and its temporal evolution, this behavior is showed to the following equation:

$$\ln(dX/dt)_{X,i} = A - \frac{\Delta E_X}{RT_{X,i}} \tag{8}$$

Dynamic mechanical analysis (DMA) of PLA/SiO$_2$ nanocomposites

Viscoelastic properties were measured using a dynamic mechanical analyzer (DMA-8000 Perkin-Elmer) in tension mode with displacement amplitude of 0.1 mm under constant strain. Specimens used were rectangular sheets measuring 2.5 mm in width, 0.5 mm in thickness and 22 mm in length. The temperature dependence of the storage modulus, loss modulus and Tan δ (phase angle δ is the difference between the dynamic tension and dynamic deformation of a viscoelastic material subjected to a sinusoidal oscillation and allows for the observation of transitions, such as T_g, in which the value of Tan δ against the temperature is 0, i.e., where one can observe a maximum on the graph) was measured at 10 across a temperature range from 30 to 100 ºC at a heating rate of 3 ºC/min. To avoid discrepancies in estimation of T_g, the

equipment software provided by Perkin-Elmer was used to calculate the transition. The purpose of this analysis was to obtain information regarding with the influence of the organic coating on the integration of particles into polymeric matrix.

Mechanical properties of films

The mechanical test consisted of tension test for the determination of the stress at break and the elasticity modulus. To determinate the tensile strength of films, the test were performed according to the ASTM standard method, D-8822-09 (ASTM, 2009) on a TAXT texture machine Plus (Stable Micro System Ltd., UK). Young's modulus and the tensile stress of PLA/SiO$_2$ nanocomposites were performed in a universal machine (Instron 3369). A 50 kN load was used maintaining a rate of 25 mm/min.

Results

Z potential and size particle

To corroborate the chemical modification made on silicon dioxide nanoparticles, Z potential tests in the pH range of 3 to 11 were performed. Changes in the Z potential are due to the nanoparticle surface charge. Highly negative or positive Z potential values suggest good colloidal stability in aqueous solutions [31]. That is, a higher surface charge implies a high repulsion between nanoparticles; so in polar matrices good behavior is expected. As seen in Fig. 1, the nanoparticles chemical modification was effective due to the change in the Z potential of samples. In Fig. 1a, it can be seen that at pH 7 values, charges are balanced in three samples. In addition, it is observed that the isoelectric point displacement is influenced by the coupling agent amount on the surface. Figure 1b shows similar behavior in three samples, this due to the surface area is large and crosslink sites are not affected by the coupling agent amount used, which is produced to a similar isoelectric point shift in porous nanoparticle specimens. In both silicon dioxide types, the presence of amino groups on
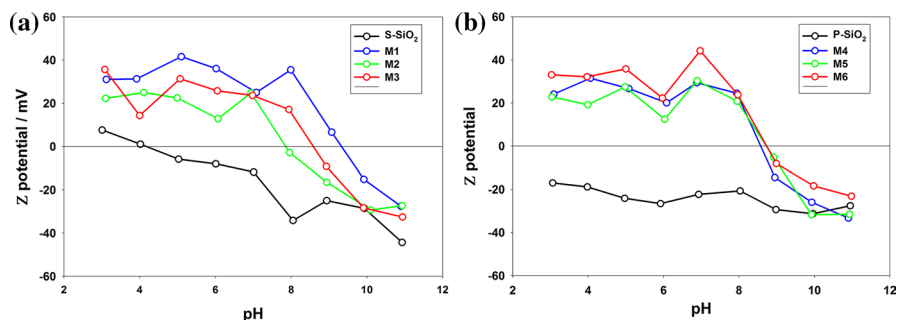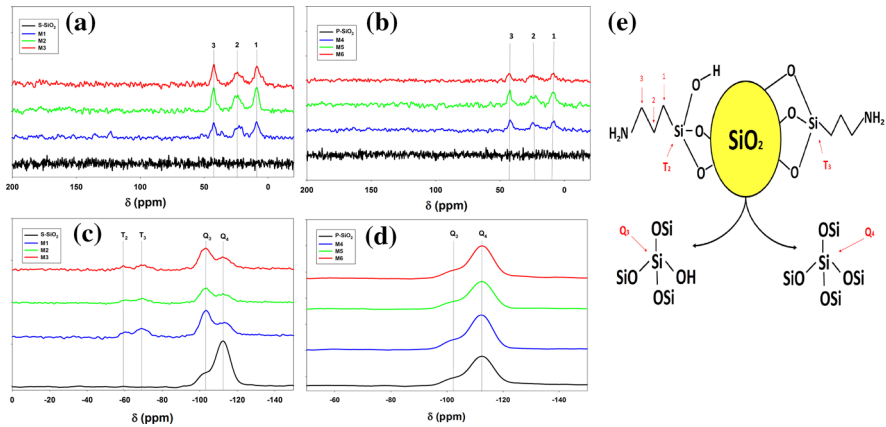

Fig. 1 Z potential of different modified and unmodified silicon dioxide nanoparticles

Table 2 Size of different modified and unmodified silicon dioxide nanoparticles

Sample	Size (mm)
S-SiO$_2$	1.99
M1	2.51
M2	1.72
M3	0.93
P-SiO$_2$	0.36
M4	1.39
M5	1.91
M6	2.85

Fig. 2 Nuclear magnetic resonance of different modified and unmodified silicon dioxide nanoparticles employed in this study

the surface implies a high dispersion in the polymer matrix of PLA. Surface modifications of metal oxides to improve their stability in biopolymer films have already been reported a better results, mainly in mechanical properties when low percentages of silanized particles are used [32].

Table 2 shows particle sizes for two silicon dioxide species. On the one hand, it is observed that the size of the agglomerate in spherical nanoparticles decreases due to the coupling agent amount on the surface that promotes their dispersion. An increase in the size of agglomerates is observed in porous nanoparticles (P-SiO$_2$ series) because the amino group amount on the surface is independent of the coupling agent ratio.

Nuclear magnetic resonance of modified SiO$_2$ nanoparticles

The nuclear magnetic resonance (NMR) spectrum characterization for ^{13}C and ^{29}Si is shown in Fig. 2. Signals at 43, 23 and 9 ppm attributed to 3 carbons from the

propyl group from the coupling agent are shown in Fig. 2a, b. These three carbon signals are represented and schematized as 1, 2 and 3 in Fig. 2e. The 4 signals of ^{29}Si are found in Fig. 2c, d, the first signal located at −59 ppm corresponds to silicon T_2, while the second signal found at−69 ppm belongs to silicon T_3. The third signal located at -103 ppm corresponds to a silicon Q_3 and the fourth signal located at −112 ppm belongs to a signal Q_4. The signals corresponding to silicon are schematized in Fig. 2e. In Fig. 2c, an inversion is observed in the signals Q_3 and Q_4, this means that the attaching of the coupling group is being carried out on the nanoparticle surface. The above indicates that the silane functional group replacement is performed in the –OH groups that are exposed in the silicon dioxide nanoparticle. In Fig. 2d, there is no change in signals Q_3 and Q_4 depending on the coupling material amount. However, the presence of the 3 carbons corresponding to the propyl group in Fig. 2b implies that the silane group is present in the nanoparticle, so the silanization reaction is taking place inside the silicon dioxide. The above is corroborated by the study of Z potential of porous nanoparticles (P-SiO$_2$ series) where it is observed that the nanoparticle surface charge distribution is independent of the coupling agent amount used.

Analysis of SiO$_2$ nanoparticles by scanning electron microscopy

After carrying out the organic coating on the surface of the different silicon dioxide particles, SEM micrographs of the modified nanoparticles were obtained. Figure 3 shows the morphology of the organic coatings as well as the bulk particle size histograms. The micrographs show a similar size among them, this is in agreement with the similarity of the sizes reported by the manufacturer. Histograms show that the organic coating causes the particle size to maintain invariant. However, the coupling agent could induce the folds formation on the nanoparticle surface, which are manifested as an increase in the available surface area. ImageJ software was used to estimate the size distributions in the micrographs

Non-isothermal crystallization analysis of PLA/SiO$_2$ nanocomposites

The non-isothermal behavior of the PLA and its SiO$_2$ nanocomposites were studied under different cooling rates (2.5, 5, 10 and 20 ºC/min). The temperature-dependent crystallization thermograms are shown in Fig. 4. Crystallization thermograms begin to widen and tend to move at higher temperatures as the cooling rate increases. The crystallization phenomenon is a process in which polymer chains tend to form ordered domains, known as crystalline domains. These domains are formed due to the polymer chains have to enter a crystalline network with an increase in the energy of the medium. It is observed in Fig. 3 that having low cooling rates (φ), nucleation centers will be formed in relatively long times. That is, there is not enough time to have stable nucleation centers at high temperatures in all specimens. It is appreciated that the thermal behavior is similar in all samples having small variations in the crystallization temperature, these data are displayed in Tables 3 and 4.
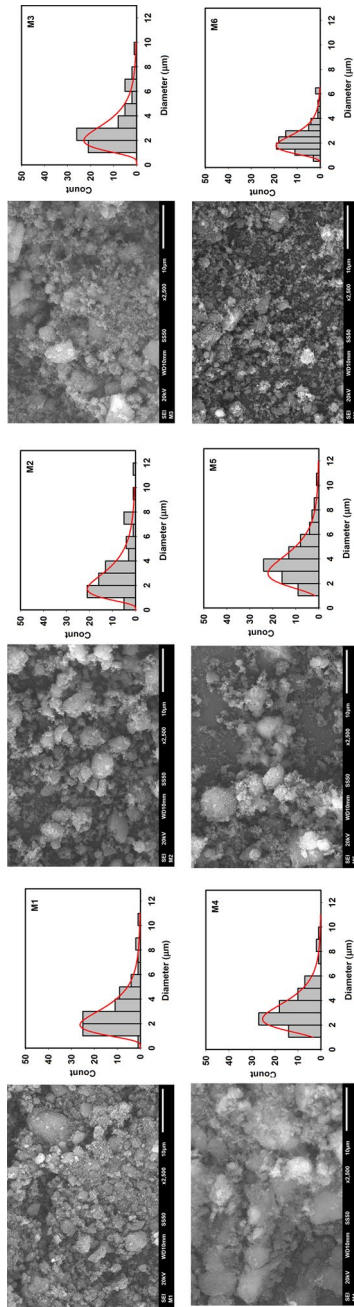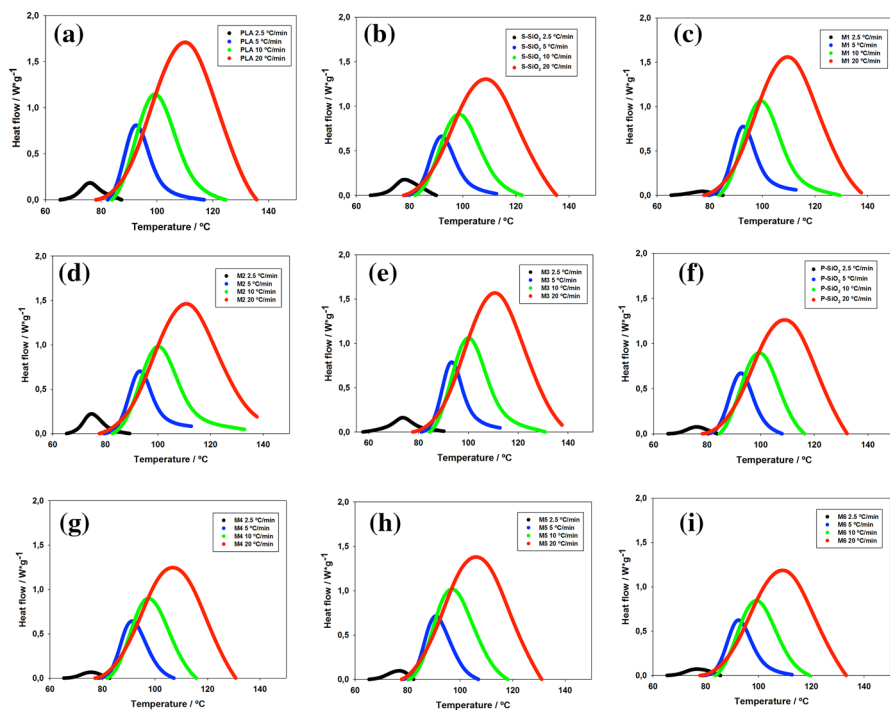
Fig. 3 SEM micrographs and size histograms for modified SiO2 nanoparticles

Fig. 4 Non-isothermal crystallization thermograms for composites of neat PLA and its nanocomposites under different crystallization cooling rates

The crystallization kinetics was achieved by integrating the thermograms of the nanocomposites. The temperature behavior appears to correlate with time owing to the functionality between the temperature of nanocomposites and the period necessary to reach the crystalline state. The stages of crystallinity in nanocomposites made up of silanized particles of varied coupling agent ratio and different surface area are shown in Fig. 5.

The obtained crystallization period (t_c) for different crystallinity stages as well as the apparent crystallization period (Δt_c) are grouped in Tables 3 and 4. The parameter Δt_c can be deduced by the discrepancy between the apparent beginning and the end while the crystallization temporal evolution occurs.

A dainty change in the non-isothermal crystallization process of the polymer was observed when it was reinforced with the nanoparticles. In addition, the required time during the crystallization process was shortened when a cooling rate of 5 ℃ min⁻¹ was maintained. While, at high cooling rates, the crystallization time evolution remained unchanged. It should be noted that the unmodified and modified SiO_2 nanoparticles act as nucleation centers, since they promote the process and increase the crystal formation rate. However, also the crystalline part of the polymer begins to be arranged and to constitute its own nucleation centers when this type of materials are subjected to a controlled temperature drop. The absence of sufficient time in all the nanocomposites was considered to appreciate the crystallization phenomenon

Table 3 Effect of cooling rate under the non-isothermal process for tested composites (part 1)

ϕ/°C min⁻¹	X=0.01	X=0.1	X=0.2	X=0.3	X=0.4	X=0.5	X=0.6	X=0.7	X=0.8	X=0.9	X=0.99	Δ t_c/min	T_p/°C	Δ H_c/Jg⁻¹
Neat PLA						t_c/min								
2.5	1.030	2.620	3.320	3.810	4.233	4.650	5.103	5.650	6.377	7.383	9.043	8.013	75.990	8.991
5	0.327	1.090	1.467	1.750	2.007	2.260	2.533	2.853	3.300	4.123	6.617	6.290	92.490	23.230
10	0.233	0.783	1.067	1.283	1.477	1.667	1.863	2.090	2.377	2.853	4.177	3.943	99.260	25.200
20	0.403	0.893	1.127	1.300	1.453	1.593	1.737	1.887	2.060	2.293	2.730	2.327	110.030	27.100
ϕ/°C min⁻¹	X=0.01	X=0.1	X=0.2	X=0.3	X=0.4	X=0.5	X=0.6	X=0.7	X=0.8	X=0.9	X=0.99	Δ t_c/min	T_p/°C	Δ H_c/Jg⁻¹
S-SiO₂/PLA						t_c/min								
2.5	1.397	3.270	4.040	4.573	5.033	5.483	5.957	6.483	7.110	7.920	9.283	7.887	78.110	9.173
5	1.023	1.850	2.230	2.513	2.767	3.010	3.267	3.560	3.930	4.507	6.013	4.990	92.020	18.330
10	0.300	0.873	1.163	1.387	1.590	1.787	1.993	2.230	2.533	3.020	4.357	4.057	98.550	21.810
20	0.350	0.830	1.070	1.247	1.403	1.553	1.700	1.857	2.043	2.290	2.743	2.393	108.560	22.620
ϕ/°C min⁻¹	X=0.01	X=0.1	X=0.2	X=0.3	X=0.4	X=0.5	X=0.6	X=0.7	X=0.8	X=0.9	X=0.99	Δ t_c/min	T_p/°C	Δ H_c/Jg⁻¹
M1/PLA						t_c/min								
2.5	0.823	2.467	3.353	4.010	4.563	5.080	5.610	6.197	6.887	7.780	9.237	8.413	77.220	3.285
5	0.883	1.703	2.070	2.340	2.577	2.807	3.050	3.323	3.673	4.223	5.697	4.813	92.690	18.510
10	0.270	0.833	1.113	1.330	1.523	1.710	1.903	2.123	2.407	2.877	4.213	3.943	99.490	22.160
20	0.390	0.880	1.113	1.290	1.440	1.583	1.727	1.880	2.057	2.293	2.740	2.350	109.560	23.800

Table 3 (continued)

ϕ/°C min^{-1}	$X=0.01$	$X=0.1$	$X=0.2$	$X=0.3$	$X=0.4$	M2/PLA tc/min $X=0.5$	$X=0.6$	$X=0.7$	$X=0.8$	$X=0.9$	$X=0.99$	Δ tc/min	Tp/°C	ΔHc/Jg^{-1}
2.5	0.950	2.317	2.917	3.350	3.733	4.110	4.510	4.967	5.547	6.460	8.633	7.683	74.750	9.984
5	0.903	1.757	2.130	2.400	2.640	2.867	2.107	3.377	3.720	4.267	5.710	4.807	93.140	17.970
10	0.347	0.950	1.240	1.457	1.650	1.837	2.030	2.247	2.527	2.977	4.263	3.917	100.140	21.610
20	0.413	0.917	1.153	1.327	1.480	1.620	1.763	1.913	2.087	2.317	2.747	2.333	110.790	23.020

ϕ/°C min^{-1}	$X=0.01$	$X=0.1$	$X=0.2$	$X=0.3$	$X=0.4$	M3/PLA tc/min $X=0.5$	$X=0.6$	$X=0.7$	$X=0.8$	$X=0.9$	$X=0.99$	Δ tc/min	Tp/°C	ΔHc/Jg^{-1}
2.5	1.297	3.593	4.690	5.393	5.937	6.417	6.900	7.450	8.163	9.330	11.787	10.490	73.730	8.742
5	0.690	1.507	1.863	2.123	2.350	2.570	2.800	3.063	3.403	3.950	5.387	4.697	93.310	19.790
10	0.253	0.810	1.090	1.300	1.490	1.673	1.867	2.090	2.373	2.850	4.150	3.897	100.060	23.540
20	0.433	0.933	1.167	1.340	1.490	1.633	1.773	1.923	2.097	2.327	2.757	2.323	110.700	25.130

because it occurs suddenly at high cooling rates without presenting an alteration in the maximum crystallization temperature (T_p).

Non-isothermal crystallization kinetics

The unfavorable use of the Avrami and Ozawa equations has been previously seen to study the phenomenon of non-isothermal crystallization in polymeric systems. We have opted to plot the data of Eq. 3 of the Avrami model and carry out the Jeziorny fit (Eq. 4), in order to kinetically parameterize the non-isothermal crystallization process of the PLA and its nanocomposites. Table 5 summarizes the kinetic parameterization by estimating n, Z_c and Z_t. Within crystallization mechanisms, a metric considered to evaluate crystal growth is the value of n. Normally, it acquires values between one and four. Three is a suggested value to explain a three- dimensional growth, as in the case of the nanocomposites analyzed in this work. These nanocomposites exhibited an increasing behavior for values of Z_c when an ascending value of φ is preserved for each of the samples. The above suggests that the crystallization rate is higher when a faster φ is evaluated as opposed to when a slower φ are used. It should be noted that notwithstanding the use of both nanoparticles series, pure PLA showed higher crystallization rates.

By applying Eq. 6 to the crystallization data, we obtained a good linear dependence between ln F(T) and ln φ. This observation confirms the applicability of the Mo model to PLA and its nanocomposites (modified and unmodified silicon dioxide nanoparticles). The results are shown in Table 6 and Fig. 6. It can be seen in Fig. 6a that the nanocomposites M1 and M3 together with the neat PLA show similar crystallization rates when the relative crystallinity reaches 0.70. By outperforming this value, the M3 nanocomposite improves its crystallization rate. It is also appreciated that the S-SiO$_2$ and M2 nanocomposites present low crystallization rates compared to pure PLA, with the M2 nanocomposite presenting a lower nucleating capacity in PLA. In Fig. 6b, we observe that the nanocomposites maintain their crystallization rate until a relative crystallinity of 0.50 is reached. Outstripping this value, we observe that the crystallinity rate of the M5 nanocomposite decreases. These results indicate that the nucleation capacity decreases when a 10:2 ratio of coupling agent is used on the silicon dioxide surfaces.

Effective activation energy from non-isothermal analysis

The reference on the effect of adding SiO$_2$ nanoparticles to the polymer matrix was obtained by the Friedman isoconvertional method (Eq. 8) based on the non-isothermal crystallization data. Through this method, we can visualize in energy terms the impact of the inclusion of modified and unmodified nanoparticles in the crystallization process through the behavior of the activation energy. This effect on crystallization can be seen in Fig. 7.

The crystallization process rate is determined by an important parameter named activation energy [33]. This parameter is the energy required to transport molecular

Table 4 Effect of cooling rate under the non-isothermal process for tested composites (part 2)

P-SiO$_2$/PLA tc/min

ϕ/°C min⁻¹	X=0.01	X=0.1	X=0.2	X=0.3	X=0.4	X=0.5	X=0.6	X=0.7	X=0.8	X=0.9	X=0.99	Δtc/min	Tp/°C	ΔHc/Jg⁻¹
2.5	0.973	2.573	3.347	3.927	4.443	4.950	5.487	6.097	6.823	7.733	9.210	8.237	76.050	6.391
5	0.653	1.457	1.830	2.110	2.353	2.590	2.833	3.113	3.463	4.017	5.447	4.793	92.540	18.720
10	0.217	0.747	1.027	1.243	1.437	1.623	1.823	2.047	2.330	2.790	4.103	3.887	99.390	21.680
20	0.417	0.900	1.133	1.310	1.463	1.607	1.750	1.903	2.083	2.320	2.763	2.347	108.880	22.230

M4/PLA tc/min

ϕ/°C min⁻¹	X=0.01	X=0.1	X=0.2	X=0.3	X=0.4	X=0.5	X=0.6	X=0.7	X=0.8	X=0.9	X=0.99	Δtc/min	Tp/°C	ΔHc/Jg⁻¹
2.5	0.927	2.447	3.207	3.783	4.303	4.810	5.347	5.963	6.707	7.660	9.193	8.267	75.700	5.859
5	0.950	1.773	2.147	2.433	2.690	2.947	3.217	3.523	3.907	4.487	5.950	5.000	91.320	20.270
10	0.283	0.830	1.110	1.323	1.513	1.700	1.893	2.107	2.367	2.743	3.600	3.317	97.480	21.350

M5/PLA tc/min

ϕ/°C min⁻¹	X=0.01	X=0.1	X=0.2	X=0.3	X=0.4	X=0.5	X=0.6	X=0.7	X=0.8	X=0.9	X=0.99	Δtc/min	Tp/°C	ΔHc/Jg⁻¹
2.5	0.860	2.400	3.173	3.740	4.227	4.677	5.117	5.577	6.113	6.903	8.767	7.907	76.940	6.468
5	0.857	1.673	2.047	2.330	2.590	2.847	3.123	3.437	3.837	4.430	5.970	5.113	90.760	20.240
10	0.340	0.907	1.197	1.423	1.630	1.833	2.050	2.300	2.617	3.123	4.493	4.153	96.870	23.950
20	0.297	0.747	0.980	1.160	1.317	1.467	1.617	1.780	1.970	2.230	2.713	2.417	106.040	24.010

Table 4 (continued)

$\phi/°C\ min^{-1}$	$X=0.01$	$X=0.1$	$X=0.2$	$X=0.3$	$X=0.4$	M6/PLA tc/min							Δ tc/min	Tp/°C	Δ Hc/Jg^{-1}
						$X=0.5$	$X=0.6$	$X=0.7$	$X=0.8$	$X=0.9$	$X=0.99$				
2.5	0.980	2.637	3.443	4.057	4.607	5.147	5.693	6.273	6.947	7.820	9.260	8.280	76.720	5.919
5	0.953	1.780	2.153	2.433	2.680	2.920	3.173	3.460	3.823	4.383	5.837	4.883	92.400	17.770
10	0.237	0.787	1.073	1.293	1.490	1.683	1.887	2.117	2.407	2.877	4.180	3.943	99.180	21.120
20	0.383	0.863	1.100	1.277	1.433	1.577	1.723	1.877	2.057	2.297	2.743	2.360	109.130	21.650
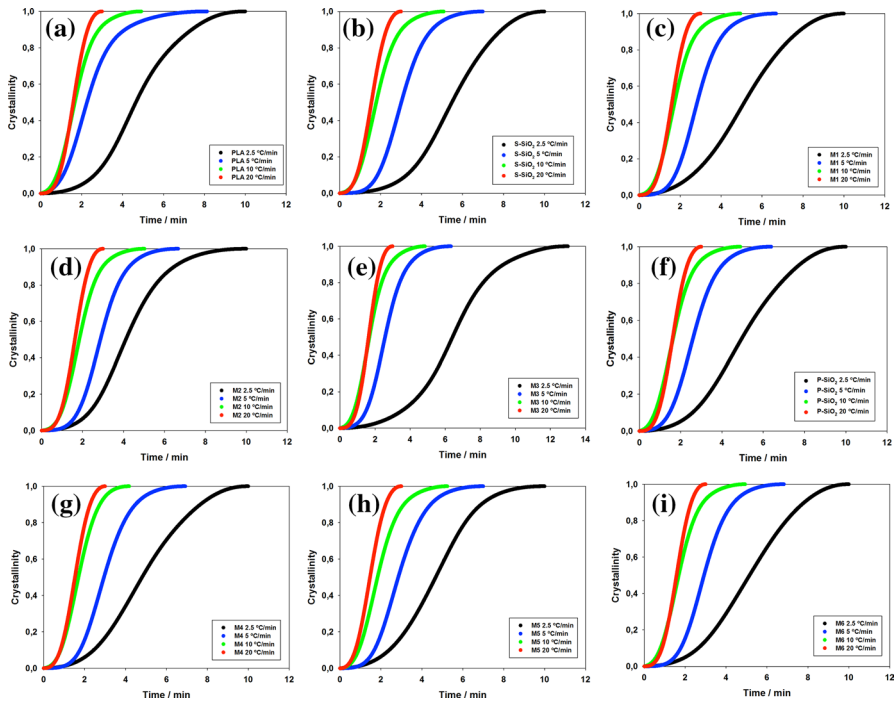
Fig. 5 Relative crystallinity behavior of PLA and its nanocomposites as function of crystallization time

segments to the surface in crystallization process. The crystallization rate is determined by two main factors: nucleation and molecular mobility of polymer chains [34, 35]. The activation energy is interpreted as the ease that materials have to form crystals or the energy necessary for the chains of material to accommodate. Figure 6a–b shows that when unmodified nanoparticles are added, there is a higher activation energy value than neat PLA, in other studies a similar behavior has been observed and suggests that nanoparticles have an effect on the PLA crystal growth [36]. Sample M2 (see Fig. 7a) shows a value slightly below the PLA, which indicates an increase in the crystallization rate of PLA. It is also observed that in percentages less than 50% crystallinity, the incorporation of modified nanoparticles (M1 and M3) avoids PLA chains to order perhaps due to a molecular mobility restriction. Similarly, we observed that at the crystallization process beginning with P-SiO$_2$ series samples, the crystal growth of PLA is prevented (see Fig. 7b). However, the behavior is maintained with slight variations, which suggests that the coating from filler does not have a significant effect on the growth of PLA crystals. Which has an advantage in terms of PLA processing.

**Table 5** Non-isothermal kinetic parameters from the Jeziorny model for PLA and its composites with $S\text{-}SiO_2$ and $P\text{-}SiO_2$

Sample	ϕ/C min^{-1}	n	Zc	Zt
PLA	2.5	3.003	0.132	0.006
	5	2.362	0.624	0.094
	10	2.430	0.849	0.195
	20	3.271	0.910	0.151
	2.5	3.501	0.078	0.002
$S\text{-}SiO_2$	5	3.459	0.428	0.014
	10	2.514	0.830	0.156
	20	3.050	0.918	0.182
	2.5	2.722	0.148	0.008
M1	5	3.411	0.454	0.019
	10	2.532	0.839	0.173
	20	3.227	0.912	0.157
	2.5	3.040	0.151	0.009
M2	5	3.502	0.439	0.016
	10	2.746	0.813	0.126
	20	3.330	0.906	0.139
	2.5	3.436	0.067	0.001
M3	5	3.234	0.498	0.031
	10	2.498	0.845	0.185
	20	3.372	0.904	0.133
	2.5	2.787	0.143	0.008
$P\text{-}SiO_2$	5	3.070	0.513	0.036
	10	2.388	0.857	0.213
	20	3.253	0.909	0.148
	2.5	2.688	0.158	0.010
M4	5	3.288	0.450	0.019
	10	2.597	0.839	0.172
	20	2.996	0.922	0.195
	2.5	2.973	0.139	0.007
M5	5	3.130	0.476	0.024
	10	2.506	0.824	0.145
	20	2.826	0.930	0.236
	2.5	2.819	0.136	0.007
M6	5	3.418	0.441	0.017
	10	2.420	0.848	0.191
	20	3.161	0.914	0.162

Dynamic mechanical analysis of PLA/SiO$_2$ films

Figure 8 shows the effect of temperature on the storage modulus and damping factor of the neat PLA and various composites with $S\text{-}SiO_2$ (a, c) and $P\text{-}SiO_2$ (b,d) with

Table 6 Non-isothermal kinetic parameters from the Mo model for PLA and its composites with S-SiO$_2$ and P-SiO$_2$

X_t/%	10	30	50	70	90
PLA					
F(T)	6.673	11.799	16.979	23.831	42.224
a	1.075	1.200	1.281	1.332	1.434
S-SiO$_2$					
F(T)	11.462	20.739	30.114	42.098	67.762
a	1.308	1.439	1.516	1.565	1.641
M1					
F(T)	8.381	14.382	19.317	25.154	39.885
a	1.236	1.256	1.270	1.283	1.370
M2					
F(T)	12.730	27.883	43.948	63.880	96.641
a	1.859	2.000	2.054	2.058	1.994
M3					
F(T)	7.877	11.693	14.910	18.992	27.358
a	0.922	0.944	0.988	1.036	1.095
P-SiO$_2$					
F(T)	7.338	12.743	17.409	22.920	35.838
a	1.118	1.203	1.233	1.248	1.324
M4					
F(T)	8.406	14.880	20.532	26.924	38.629
a	1.216	1.309	1.331	1.332	1.349
M5					
F(T)	9.116	16.676	24.143	35.838	70.386
a	1.393	1.435	1.479	1.561	1.740
M6					
F(T)	8.077	13.943	19.011	25.330	40.977
a	1.101	1.208	1.240	1.272	1.375
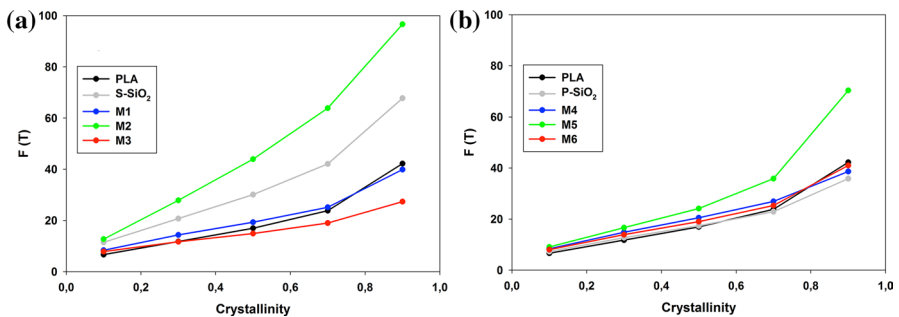
Fig. 6 F(T) versus crystallinity behavior of PLA and its composites with **a** S-SiO$_2$ and **b** P-SiO$_2$

different 3-APTMS content on the silicon dioxide surface. Variation in modulus occurs owing to the effect of the incorporated filler.

Figure 8a indicates that nanocomposites (S-SiO$_2$ series) have a larger storage modulus than pure PLA. Firstly, when S-SiO$_2$ was added with a surface modification of 3-APTMS with a 10:2 ratio (M2), there was a significant increase. Furthermore, it was observed that the incorporation of S-SiO$_2$ with the least amount of coupling agent maintains similar the behavior of the virgin PLA matrix. Also, we observed that the incorporation of the unmodified nanoparticle (S-SiO$_2$) had an improvement in the storage modulus of PLA. This is because it is known that using spherical mineral fillers tends to increase the storage modulus due to the stiffness of the filler [37].

Figure 8b shows that some of nanocomposites (P-SiO$_2$ series) have a smaller storage modulus than pure PLA. It is again observed that when P-SiO$_2$ was added with a 3-APTMS surface modification with 10:2 ratio (M5), there was a significant increase, although less than in the M2 sample. Furthermore, it was observed that the incorporation of P-SiO$_2$ with the least amount of coupling agent (M6) maintains a similar behavior of the PLA virgin matrix. Furthermore, we observed that the incorporation of the unmodified nanoparticle (P-SiO$_2$), as well as the sample with high load of coupling agent (M4), had a decrease in the PLA storage module. This could be caused by agglomeration of nanoparticles in the PLA matrix. Increasing the storage modulus, as shown in Fig. 8a, b, suggests that there may be an optimal coupling agent concentration on the surface to enhance the interaction between the PLA polymer and silica nanoparticles (samples M2 and M5).

The damping properties improvement is related to the appearance of a higher degree of molecular mobility by the polymer chains. This mobility is reflected in an increase in the area under the behavior curve of Tan δ [38]. The area under the α-relaxation peak in conformed PLA nanocomposites is approximately 60° C (see Fig. 8c–d). The area appears to widen without affecting the maximum temperatures for nanocomposites that are reinforced with nanoparticles without actually showing a specific trend regarding the coupling agent increase on the nanoparticle surface [39]. The glass transition temperature (T_g) is influenced by factors such as the nanoparticle surface and even by the dispersion along the polymer matrix [40]. In
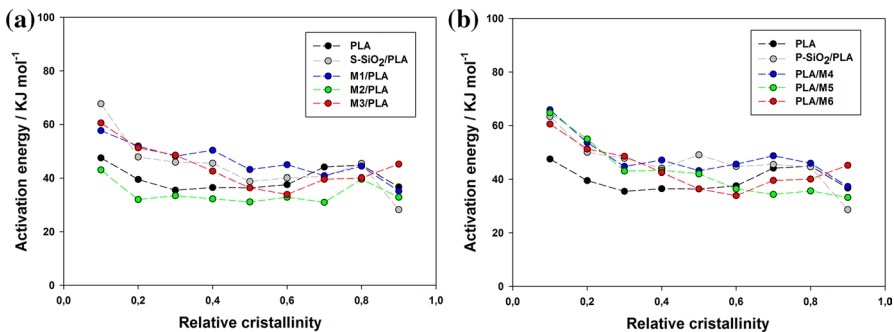

Fig. 7 Activation energy behavior as function of crystallinity degree for PLA and its nanocomposites. **a** S-SiO$_2$ series and **b** P-SiO$_2$ series

addition to this, there are studies where polymer–nanoparticle interactions play an important role in the polymers dynamics, mainly when they are in the molten state [41]. In Fig. 8c–d, it is observed that the T_g in both nanocomposites series is independent of the coupling agent amount on the silicon dioxide surface; other authors who have worked with silicon dioxide have reported similar behaviors [42]. The addition of porous silicon dioxide nanoparticles (P-SiO$_2$ series) in the PLA matrix shows two Tan δ peaks for some composites (P-SiO$_2$, M4 and M5) (see Fig. 8) and is appreciates that the second peak decreases as the amount of coupling agent decreases. This second peak can be attributed to the formation of a crosslinked microgel structure to the PLA matrix [43].

Mechanical properties of PLA/SiO$_2$ films

Table 7 shows mechanical properties, including tensile stress and Young's modulus of pure PLA and its nanocomposites (S-SiO$_2$ and P-SiO$_2$ series). In this study, Young's modulus and stress values for the pure PLA were 15.90 MPa and 1000.70 MPa, respectively. PLA had an increase in tensile stress when unmodified spherical silicon dioxide nanoparticles (S-SiO$_2$) were added. Furthermore, an increase in tensile stress was noted when the coupling agent amount on the surface decreased, achieving an improvement of 40.25% for M3 sample. PLA
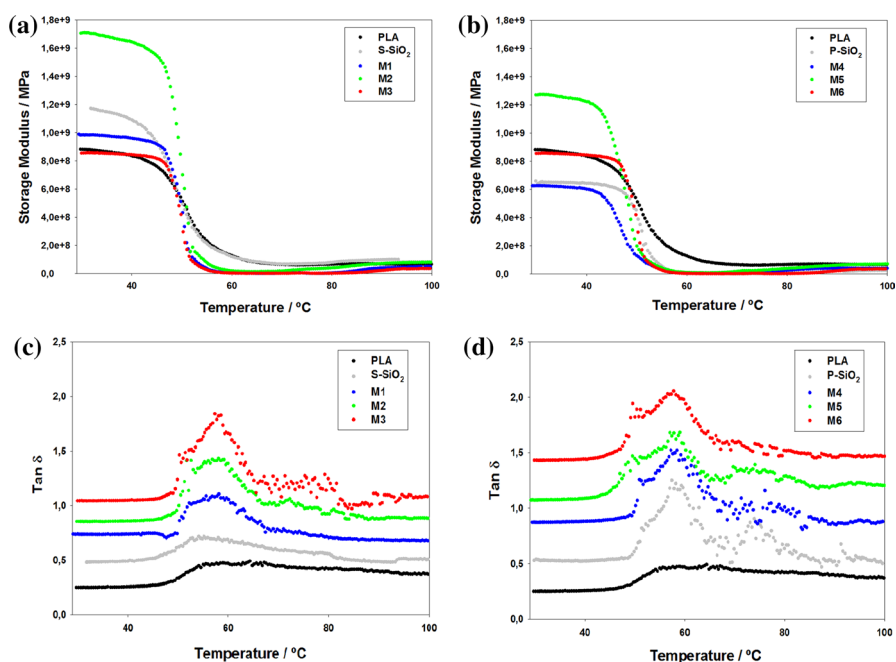
Fig. 8 Dynamic mechanical analysis (DMA) storage modulus curves of **a** PLA/S-SiO$_2$ and **b** PLA/P-SiO$_2$ composites. Dynamic mechanical analysis (DMA) damping factor curves of **c** PLA/S-SiO$_2$ and d) PLA/P-SiO$_2$ composites

nanocomposites of P-SiO$_2$ series were maintained in a range of 15–17 MPa, indicating that the incorporation of this nanomaterial has tiny effect on tensile stress. However, the decrease in tensile stress in these nanomaterials was around 7%. This decrease can be attributed to a hydrolytic degradation of PLA. Other authors have proposed that the incorporation of nanomaterials (such as carbon nanotubes and silica nanoparticles) can accelerate the hydrolytic degradation of PLLA [44, 45].

S-SiO$_2$ nanoparticles series incorporated in the PLA matrix improve Young's modulus to a maximum point of 1352.55 MPa for the M2 sample. This represents an improvement of 35.16% with respect to the PLA matrix. The improvement range is 17.94–35.16%, which makes the nanocomposite ideal for applications where a resistant material is required using this filler. The opposite effect in improving the resistance of the PLA matrix occurs when P-SiO$_2$ nanoparticles series are incorporated. There are decreases in Young's modulus with respect to the PLA between 10.59 and 51.97%. According to the results obtained with respect to Young's modulus, a trend is seen considering the specific surface area values shown in Table 1. As the surface area increases, the Young's modulus is diminished. This indicates that the material has a better elasticity and makes a difference in the effect of surface area and the coupling agent amount found on the nanomaterial surface.

Conclusions

In this research work, the effect of the surface area of silicon dioxide nanoparticles and their polarity change by means of a coupling agent on mechanical and thermal properties of PLA nanocomposites was evaluated. Within this, it was demonstrated that changing the dose of compatibilizer modifies the isoelectric point of nanoparticles, which indicates that it charges differently. When introducing them into a polymer, changes in mechanical properties were observed through an increase in elasticity when nanoparticles with high surface area were used, and an increase in stiffness when nanoparticles with low surface area were employed, reaching a maximum in the 10:2 ratio of coupling agent.

Table 7 Mechanical tests for PLA and its composites with S-SiO$_2$ and P-SiO$_2$

Sample	Tensile stress (MPa)	Young's modulus (MPa)
PLA	15.90	1000.70
S-SiO$_2$/PLA	17.37	1282.33
M1/PLA	19.51	1180.26
M2/PLA	21.83	1352.55
M3/PLA	22.30	1315.17
P-SiO$_2$/PLA	14.97	744.89
M4/PLA	12.47	480.62
M5/PLA	16.37	598.62
M6/PLA	17.34	894.73

In dynamic mechanical properties, it was observed an increase in the storage modulus for both types of nanoparticles when a 10:2 ratio is used again. The glass transition temperature was kept constant and in thermal properties an increase in the crystallization rate was observed for the 10:2 ratio in both nanoparticles; there were differences when using spherical nanoparticles and a low rate disturbance when using nanoparticles with a high surface area. Finally, it was shown that the surface area does not play a role in the energy required for crystal formation but has a direct effect on mechanical properties as discussed above.

According to their Young's modulus, the most rigid nanocomposites were those made with spherical nanoparticles, presenting an optimum when the coupling agent ratio is 10:2. In dynamic mechanical properties, for both samples regardless of the surface area, the 10:2 ratio showed a better performance, which is consistent with crystallization rates. We observe that the rate of crystal formation plays an important role in mechanical properties of formed nanocomposites by nanoparticles with low surface area. On the other hand, when nanocomposites are reinforced with high surface area nanoparticles, the amount of formed crystals is what influences mechanical properties of nanocomposites; this due to polymer chains have a different arrangement around nucleation centers.

References

1. Nabi Saheb D, Jog JP (1999) Natural fiber polymer composites: a review. Adv Polymer Technol J Polymer Process Inst 18(4):351–363
2. Lim L-T, Auras R, Rubino M (2008) Processing technologies for poly (lactic acid). Progress Polymer Sci 33(8):820–852
3. Sengupta S, Manna S, Roy U, Das P (2018) Manufacturing of biodegradable poly lactic acid (pla): green alternatives to petroleum derived plastics. In: Reference module in materials science and materials engineering. Encyclopedia of renewable and sustainable materials, vol 3. Elsevier, pp 561–569
4. Wang G, Zhang D, Wan G, Li Bo, Zhao G (2019) Glass fiber reinforced pla composite with enhanced mechanical properties, thermal behavior, and foaming ability. Polymer 181:121803
5. Suryanegara L (2009) Antonio Norio Nakagaito, and Hiroyuki Yano 2009 The effect of crystallization of pla on the thermal and mechanical properties of microfibrillated cellulose-reinforced pla composites. Compos Sci Technol 69:1187–1192
6. Chen P-Y, Lian H-Y, Shih Y-F, Chen-Wei S-M, Jeng R-J (2017) Preparation, characterization and crystallization kinetics of kenaf fiber/multi-walled carbon nanotube/polylactic acid (pla) green composites. Mater Chem Phys 196:249–255
7. Hung C-Y, Wang C-C, Chen C-Y (2013) Enhanced the thermal stability and crys- tallinity of poly-lactic acid (pla) by incorporated reactive ps-b-pmma-b-pgma and ps-b-pgma block copolymers as chain extenders. Polymer 54(7):1860–1866
8. Garcia CV, Shin GH, Kim JT (2018) Metal oxide-based nanocomposites in food packaging: applications migration and regulations. Trends Food Sci Technol 82:21–31

9. Shankar S, Wang L-F, Rhim J-W (2018) Incorporation of zinc oxide nanoparticles improved the mechanical, water vapor barrier, uv-light barrier, and antibacterial properties of pla- based nanocomposite films. Mater Sci Eng, C 93:289–298

10. Sarikhani K, Nasseri R, Lotocki V, Thompson RB, Park CB, Chen P (2016) Effect of well-dispersed surface-modified silica nanoparticles on crystallization behavior of poly (lactic acid) under compressed carbon dioxide. Polymer 98:100–109

11. Vandenberg ET, Bertilsson L, Liedberg B, Uvdal K, Erlandsson R, Elwing H, Lundström I (1991) Structure of 3-aminopropyl triethoxy silane on silicon oxide. J Colloid Interface Sci 147(1):103–118

12. Vallejo-Montesinos J, Gámez-Cordero J, Zarraga R, Pérez MCP, Gonzalez-Calderon JA (2020) Influence of the surface modification of titanium dioxide nanoparticles TiO$_2$ under efficiency of silver nanodots deposition and its effect under the properties of starch–chitosan (sc) films. Polymer Bull 77(1):107–133

13. López-Zamora L, Martínez-Martínez HN, González-Calderón JA (2018) Improvement of the colloidal stability of titanium dioxide particles in water through silicon based coupling agent. Mater Chem Phys 217:285–290

14. Gonzalez-Calderon JA, Mendoza G, Peña-Juárez MG, Pérez E et al (2020) Use of chemically modified titanium dioxide particles to mediate the non-isothermal cold crystallization of poly (latic acid). J Mexican Chem Soc 64(2):117–136

15. Knowles GP, Graham JV, Delaney SW, Chaffee AL (2005) Aminopropyl- functionalized mesoporous silicas as co2 adsorbents. Fuel Process Technol 86:1435–1448

16. Jaksa G, Štefane B, Kovač J (2014) Influence of different solvents on the morphology of aptms-modified silicon surfaces. Appl Surf Sci 315:516–522

17. Jakša G, Štefane B, Kovač J (2013) Xps and afm characterization of aminosilanes with different numbers of bonding sites on a silicon wafer. Surf Interface Anal 45(11–12):1709–1713

18. Saeidlou S, Huneault MA, Li H, Park CB (2012) Poly (lactic acid) crystallization. Progress Polymer Sci 37(12):1657–1677

19. Rene Androsch HM, Iqbal N, Schick C (2015) Non-isothermal crystal nucleation of poly (l-lactic acid). Polymer 81:151–158

20. As'habi L, Jafari SH, Khonakdar HA, Häussler L, Wagenknecht U, Heinrich G (2013) Non-isothermal crystallization behavior of pla/lldpe/nanoclay hybrid: synergistic role of lldpe and clay. Thermochim Acta 565:102–113

21. Chen H, Pyda M, Cebe P (2009) Non-isothermal crystallization of pet/pla blends. Ther- mochimica Acta 492(1–2):61–66

22. Li H, Huneault MA (2007) Effect of nucleation and plasticization on the crystallization of poly (lactic acid). Polymer 48(23):6855–6866

23. Nofar M, Tabatabaei A, Park CB (2013) Effects of nano-/micro-sized additives on the crystallization behaviors of pla and pla/co2 mixtures. Polymer 54(9):2382–2391

24. Tsuji H, Takai H, Fukuda N, Takikawa H (2006) Non-isothermal crystallization behavior of poly (l-lactic acid) in the presence of various additives. Macromol Mater Eng 291(4):325–335

25. Lizundia E, Penayo MC, Guinault A, Vilas JL, Domenek S (2019) Impact of zno nanoparticle morphology on relaxation and transport properties of pla nanocomposites. Polym Testing 75:175–184

26. Kissinger HE (1956) Variation of peak temperature with heating rote in differential thermal analysis. J Res NatlBureau Standards 57:217

27. Blaine RL, Kissinger HE (2012) Homer kissinger and the kissinger equation. Thermochim Acta 540:1–6

28. Vyazovkin S (2002) Is the kissinger equation applicable to the processes that occur on cooling? Macro- molecular Rapid Commun 23(13):771–775

29. Vyazovkin S, Burnham AK, Criado JM, Perez-maqueda LA, Popescu C, Sbirrazzuoli N (2011) ICTAC Kinetics Committee recommendations for performing kinetic computations on thermal analysis data. Thermochim Acta 520:1–19

30. Friedman HL (1969) New methods for evaluating kinetic parameters from thermal analysis data. J Polymer Sci Part B Polymer Lett 7(1):41–46

31. Liao DL, Wu GS, Liao BQ (2009) Zeta potential of shape-controlled tio2 nanoparticles with surfactants. Colloids Surf, A 348(1–3):270–275

32. Alvarado ED, Juárez MGP, Pérez CP, Perez E, Gonzalez JA et al (2019) Improvement in the dispersion of tio2 particles inside chitosan-methyl cellulose films by the use of silane coupling agent. J Mexican Chem Soc 63(2):154–168

33. Papageorgiou GZ, Achilias DS, Nanaki S, Beslikas T, Bikiaris D (2010) PLA nanocomposites: effect of filler type on non-isothermal crystallization. Thermochim Acta 511(1–2):129–139

34. Fernández MJ, Fernández MD (2020) Effect of organic modifier and clay content on non-isothermal cold crystallization and melting behavior of polylactide/organovermiculite nanocomposites. Polymers 12(2):364

35. Chen Y, Yao X, Qun Gu, Pan Z (2013) Non-isothermal crystallization kinetics of poly (lactic acid)/graphene nanocomposites. J Polym Eng 33(2):163–171

36. Zhang Y, Deng B, Liu Q, Chang G (2013) Nonisothermal crystallization kinetics of poly (lactic acid)/nanosilica composites. J Macromol Sci, Part B 52(2):334–343

37. Zhu A, Diao H, Rong Q, Cai A (2010) Preparation and properties of polylactide—silica nanocomposites. J Appl Polym Sci 116(5):2866–2873

38. Pilla S, Kramschuster A, Yang L, Lee J, Gong S, Turng L-S (2009) Microcellular injection-molding of polylactide with chain-extender. Mater Sci Eng, C 29(4):1258–1265

39. Mofokeng JP, Luyt AS, Tábi T, Kovács J (2012) Comparison of injection moulded natural fibre-reinforced composites with pp and pla as matrices. J Thermop Compos Mater 25(8):927–948

40. Wen X, Lin Y, Han C, Zhang K, Ran X, Li Y, Dong L (2009) Thermomechanical and optical properties of biodegradable poly (l-lactide)/silica nanocomposites by melt compounding. J Appl Polym Sci 114(6):3379–3388

41. Glotzer SC, Paul W (2002) Molecular and mesoscale simulation methods for polymer materials. Ann Rev Mater Res 32(1):401–436

42. Huang TC, Yeh JM, Yang JC (2010) Effect of silica size on the thermal, mechanical and biodegradable properties of polylactide/silica composite material prepared by melt blending. Adv Mater Res 123-125:1215–1218

43. Pothan LA, Oommen Z, Thomas S (2003) Dynamic mechanical analysis of banana fiber reinforced polyester composites. Compos Sci Technol 63(2):283–293

44. Zhao Y, Qiu Z, Yang W (2009) Effect of multi-walled carbon nanotubes on the crystallization and hydrolytic degradation of biodegradable poly (l-lactide). Compos Sci Technol 69(5):627–632

45. Jyh-Hong Wu, Yen MS, Kuo MC, Chen BH (2013) Physical properties and crystallization behavior of silica particulates reinforced poly (lactic acid) composites. Mater Chem Phys 142(2–3):726–733

Authors and Affiliations

I. Montes-Zavala[1] · M. J. Pérez-González[2] · E. O. Castrejón-González[1] · Diego A. Santamaría-Razo[3] · A. Almendárez-Camarillo[1] · E. Pérez[4] · J. A. Gonzalez-Calderon[5]

✉ J. A. Gonzalez-Calderon
    amir@ifisica.uaslp.mx

1   Departamento de Ingeniería Química, Tecnológico Nacional de México en Celaya, Av. Tecnológico Y A. García Cubas S/N, 38010 Celaya, Guanajuato, México

2   Facultad de Ciencias, Universidad Autónoma de San Luis Potosí, Av. Parque Chapultepec 1570, 78210 San Luis Potosí, México

3   Innovation Centre for Sustainable Construction, CRH Nederland B.V., Amsterdam, The Netherlands

4   Instituto de Física, Universidad Autónoma de San Luis Potosí, Zona Universitaria, Av. Manuel Nava 6, 78290 San Luis Potosí, México

5   Cátedras CONACYT-Instituto de Física, Universidad Autónoma de San Luis Potosí, Zona
    Universitaria, Av. Manuel Nava 6, 78290 San Luis Potosí, México